

Observing Ultra-High Energy Cosmic Rays with Smartphones

Daniel Whiteson,¹ Michael Mulhearn,² Chase Shimmin,¹ Kyle Brodie,¹ and Dustin Burns²

¹*Department of Physics and Astronomy, University of California, Irvine, CA 92697*

²*Department of Physics, University of California, Davis, CA*

We propose a novel approach for observing cosmic rays at ultra-high energy ($> 10^{18}$ eV) by repurposing the existing network of smartphones as a ground detector array. Extensive air showers generated by cosmic rays produce muons and high-energy photons, which can be detected by the CMOS sensors of smartphone cameras. The small size and low efficiency of each sensor is compensated by the large number of active phones. We show that if user adoption targets are met, such a network will have significant observing power at the highest energies.

PACS numbers:

Introduction

The source of ultra-high energy cosmic rays (UHECR), those with energy above 10^{18} eV, remains a puzzle even many decades after their discovery, as does the mechanism behind their acceleration. Their high energy leaves them less susceptible to bending by magnetic fields between their source and the Earth, making them excellent probes of the cosmic accelerators which produce them [1, 2]. But the mechanism and location of this enormous acceleration is still not understood, despite many theoretical conjectures [3–6].

When incident on the Earth’s atmosphere, UHECRs produce extensive air showers, which can be detected via the particle flux on the ground, the fluorescence in the air, or the radio and acoustic signatures. A series of dedicated detectors [7–9] have detected cosmic rays at successively higher energies, culminating in observation up to $3 \cdot 10^{20}$ eV. The flux of particles drops precipitously above 10^{18} GeV, due to the suppression via interaction with the cosmic microwave background [10, 11], making observation of these particles challenging.

To accumulate a sufficient number of observed showers requires either a very long run or a very large area. Constructing and maintaining a new detector array with a large effective area faces significant obstacles. Current arrays with large, highly-efficient devices (Auger [12], AGASA [13]) cannot grow dramatically larger without becoming much more expensive. Distributed detector arrays with small, cheaper devices (ERGO [14], etc) have the potential to grow very large, but have not achieved the size and density required to probe air showers, potentially due to the organizational obstacles of production, distribution and maintenance of their custom-built devices.

It has been previously shown that smartphones can detect ionizing radiation [15, 16]. In this paper, we demonstrate that a dense network of such devices has power sufficient to detect air showers from the highest energy cosmic rays. We measure the particle-detection efficiency

of several popular smartphone models, which is necessary for the reconstruction of the energy and direction of the particle initiating the shower. With sufficient user adoption, such a distributed network of devices can observe UHECRs at rates at least comparable to conventional cosmic ray observatories. Finally, we describe the operating principles, technical design and expected sensitivity of the CRAYFIS (Cosmic RAYs Found In Smartphones) detector array. Preliminary applications for Android and iOS platforms are available for testing [17].

Detection

Air showers induced by cosmic rays contain an enormous number of particles. Figure 1 shows the energy spectrum, and spatial distribution at sea level of photons, electrons, and muons in showers as simulated by the CORSIKA [18] program with the QGS-II [19] model of hadronic interactions.

We focus our attention on photons, which have high densities in the shower, and muons, which have excellent penetrating power and high detection efficiency. Electrons are also numerous and have high efficiency, but may be blocked by buildings, phone cases or camera lenses. Heavier hadronic particles are much less common.

The sensitive element in a smartphone is the camera, a CMOS device in which silicon photodiode pixels are designed to absorb visible photons and convert them to current which is collected and read out. While these devices are designed to have reasonable quantum efficiency for visible light, the same principle allows the sensor to detect higher-energy photons [15] as well. In the case of muons, the photodiode is functionally equivalent to silicon-based trackers now common in particle physics experiments, such that the charged particle will leave electron-hole pairs along its path.

A GEANT-based simulation [20] of the energy deposition of photons in silicon indicates that the camera sensor has efficiency over the energy range of interest (Fig. 2).

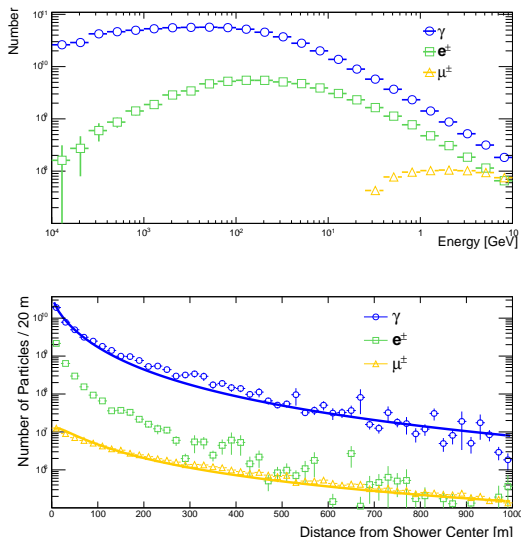


FIG. 1: Energy spectrum (a) and distance from shower axis (b) of photons, electrons, and muons at ground level for simulated air showers initiated by protons with energy $10^{19} - 10^{20}$ eV. Also shown (b) is a parametric fit to Eq 1.

Such simulations have been validated extensively in the context of silicon-strip detectors for particle physics experiments. An application running on the smartphone has access to an array of eight-bit *pixel response* values. Though many stages of processing occur between the direct measure of the deposited energy by the CMOS sensor and the delivery of pixel response values, we assume that the former is a reasonable proxy for the latter.

Software

With the camera as the detector element, the phone processor runs an application which functions as the trigger and data acquisition system. To obtain the largest possible integrated exposure time, the first-level trigger captures video frames at 15-30 Hz, depending on the frame-processing speed of the device. Frames which contain any above-threshold pixels are stored and passed to the second stage which examines the stored frames, saving only the pixels above a second, lower threshold. All qualifying pixels, typically a few per frame, are stored as a sparse array in a buffer on the phone, along with their arrival time and the geolocation of the phone. When a wi-fi connection is available, the collected pixels are uploaded to a central server for offline shower reconstruction; most events are between 50 – 200 bytes of data. The acquired event rate may be tuned by setting the thresholds to eliminate spurious background events; typical rates are 0.2 Hz.

The application runs when the phone is not in active use. It launches itself when it detects a power source,

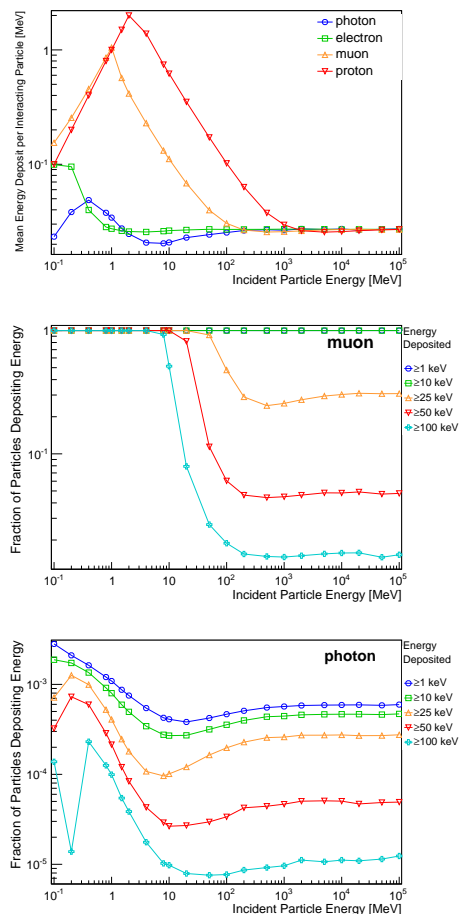


FIG. 2: Studies of energy deposition by photons, electrons and muons incident on $50\mu\text{m}$ -thick Si in GEANT simulations. The top pane shows the mean energy deposition per interacting particle; those which pass through without interacting are omitted. The center (bottom) pane shows the fraction of incident photons (muons) which deposit energy above a set of thresholds.

and quits when the power is disconnected. No additional light shielding, such as tape, of the camera is required, other than placing the phone face-up (camera-down) on a table. In this way, no active participation is required once the application is installed and its operation should be fairly inobtrusive, which is critical to achieving wide participation in the smartphone community. To address user security concerns, no frames will be stored or uploaded if the average pixel response value over the frame exceeds a threshold, such that full images cannot be reconstructed offline.

Offline, we perform hot-pixel removal. Individual pixels that fire at a rate much higher than the average are removed; these are caused either by light leakage, typically near the edge of the frame, or by poorly-performing or noisy pixels.

Photon Reconstruction and Efficiency

Detection of particles in smartphones has been performed previously [15], but application of such measurements to the observation of extensive air showers from UHECRs has not yet been explored. A critical step is understanding the product of active area and the efficiency $A\epsilon$ of each device for the particles species in an air shower. The number of events N_{cand} that pass the trigger threshold determines the efficiency $\epsilon = N_{\text{cand}}/N_{\text{incident}}$ of the device. Measurements of the efficiency are presented below, and details of A are typically available from manufacturers.

The response of several popular phone models to photons was measured in the lab using gamma rays from the radioactive decays of Ra^{226} ($E_\gamma = 30 - 600$ keV), Co^{60} ($E_\gamma = 1.2$ MeV) and Cs^{137} ($E_\gamma \leq 700$ keV). As a representative example, the measured pixel response of a Samsung Galaxy S3 is shown in Fig. 3; similar spectra are seen in other Android models as well as iPhones. In the presence of radioactive sources, the camera detects pixels with a large charge deposition at a rate that is proportional to the activity of our sources. When no source is nearby, the distribution of pixel response values presents a steeply falling distribution, with a long tail that we attribute to cosmic ray muons (see discussion below). To confirm the sensitivity of the phones to photons, we periodically place a radioactive source near a phone and remove it; Fig. 4 shows that the number of pixels with a value above a trigger threshold is highly correlated with the presence of a radioactive source. In addition to leaving isolated pixels with large pixel response values, some high energy photons leave several bright pixels in clusters or tracks; see Fig. 5. These can be attributed to compton-scattered and pair-produced electrons.

For a radioactive source with activity R a distance d from the sensor, we can measure $A\epsilon$ by counting the number of events observed N_{obs} over a period Δt :

$$A\epsilon = 4\pi d^2 \frac{N_{\text{obs}}}{R\Delta t}.$$

The activity of each radioactive source was determined using a high-precision photon counter at the UC Irvine test reactor. The distance from the camera to the source was kept constant using a wax assembly, allowing us to measure $A\epsilon$ to within a few percent. We found only minor variation in $A\epsilon$ for the different photon sources listed above. Between the different phone models tested, we measured a range of $A\epsilon$ of $2.5 \times 10^{-9} - 2.5 \times 10^{-8}$ m², with consistent values of $A\epsilon$ between phones of the same model. We therefore consider a conservative range of average photon sensitivity of $A\epsilon = (1 - 5) \times 10^{-9}$ m² for projections.

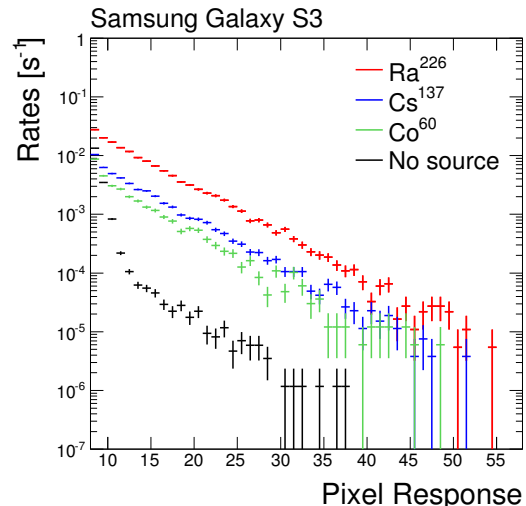


FIG. 3: Distribution of observed pixel response values in a Samsung Galaxy S3 phone when exposed to sources which emit photons between 30-1200 keV, and without any source. The differences in rates are due to the different activity of the sources. The data with no source shows a falling noise distribution and a tail attributed to cosmic muons. Other phone models show qualitatively similar behavior.

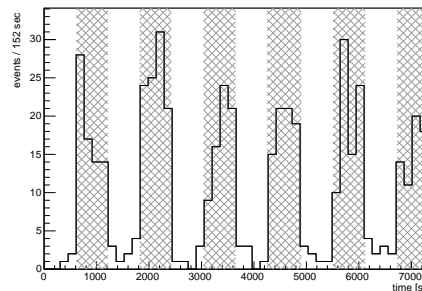


FIG. 4: Number of pixels with value above trigger threshold versus time in a Samsung Galaxy S3 phone. In the periods indicated by hatching, a ^{226}Ra source has been placed near the phone.

Muon Reconstruction and Efficiency

Muon efficiencies are measured by observing the rate of hits above the noise distribution. Measurements are made where the phone is shielded by at least 5cm of lead, to suppress contributions from ambient radioactivity. Comparison of the observed rate of muon candidates to the local cosmic ray muon rate determines the muon efficiency $\epsilon = 0.8 \pm 0.2$. In the field, device $A\epsilon$ can be determined *in situ* by calibration to cosmic muon rates. Runs at higher altitude during commercial airline flights display an increase in observed charged particle candidates, consistent with expectation. A candidate charged

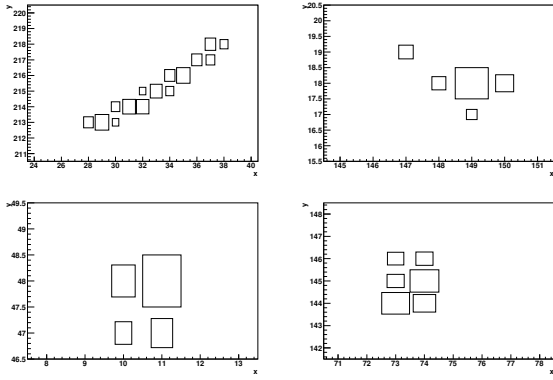


FIG. 5: Activated pixels above threshold in a Samsung Galaxy SIII phone, during exposure to ^{60}Co . Box size is proportional to pixel response values

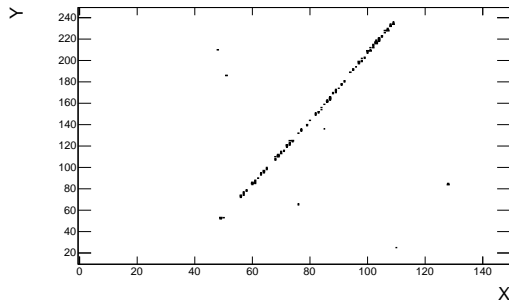


FIG. 6: Activated pixels from a charged particle observed during a commercial airline flight, at an altitude above 10km. At this altitude, it is most likely a proton.

particle event is shown in Fig. 6, showing a clear track. Although this event may be due to an energetic proton, the fact that the track has few gaps indicates that the per-pixel response to minimally-ionizing particles such as muons is highly efficient. Future measurements with coincident scintillators can provide more accurate assessments of muon efficiencies.

Shower Reconstruction

In the presence of an air shower, the local density of particles can be written as a vector $\boldsymbol{\rho}(x, y)$, where each component refers to a particular species of particle (muon or photon). A phone, with active detector element area A , and particle species identification efficiency vector $\boldsymbol{\epsilon} = (\epsilon_\mu, \epsilon_\gamma)$, will reconstruct a mean number of candidates $\lambda = \eta + A\boldsymbol{\epsilon} \cdot \boldsymbol{\rho}(x, y)$, where η is the mean background.

The probability that a phone will register no candidates is then given by the Poisson distribution:

$$P_0(x, y) = e^{-A\boldsymbol{\epsilon} \cdot \boldsymbol{\rho}(x, y) - \eta},$$

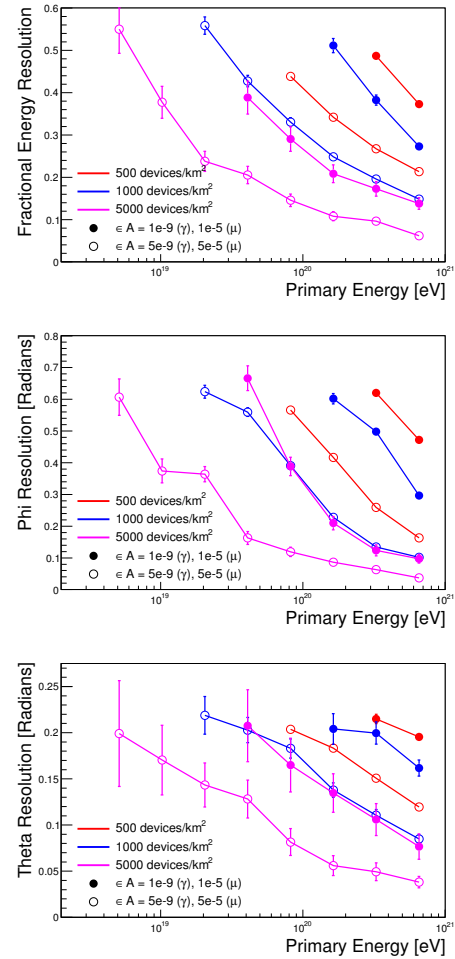


FIG. 7: Fractional energy resolution (top), and ϕ (middle) and θ (bottom) resolution in radians, for simulated events. Shown are resolutions for two choices of per-phone area times efficiency ($A\epsilon$) and three examples of user adoption density.

while the probability that the phone will register one or more candidates is:

$$P_1(x, y) = 1.0 - e^{-A\boldsymbol{\epsilon} \cdot \boldsymbol{\rho}(x, y) - \eta}.$$

If the quantity $A\epsilon$ is known for each phone and particle species type, measuring the distribution of phones with and without candidates constrains the local shower density $\rho_i(x, y)$, of each particle species i . The density is directly proportional to the incident particle energy with a distribution in x and y sensitive to the incident particle direction. We use a parameterized model for ρ [21]

$$\rho(N_i, r, s) = \frac{N_i}{2\pi r_M^2} \left(\frac{r}{r_M}\right)^{(s-2)} \left(1 + \frac{r}{r_M}\right)^{(s-4.5)} \times \left(\frac{\Gamma(4.5-s)}{\Gamma(s)\Gamma(4.5-2s)}\right) [\text{m}^{-2}] \quad (1)$$

where r is the distance of a detector element to the vec-

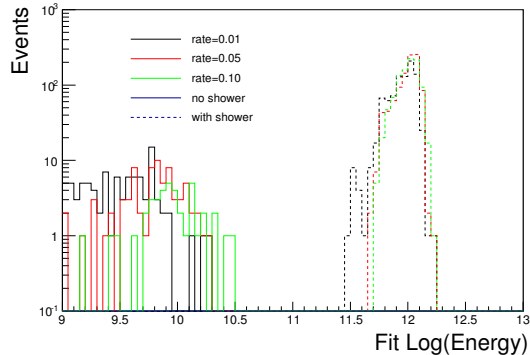


FIG. 8: Demonstration of the impact of noise hits on the measured energy of simulated showers. The reconstructed energy from events containing simulated showers (labeled ‘with shower’) is quite distinct from those consisting solely of simulated noise (labeled ‘no shower’), even for very high noise rates varying from 1% to 10% of phones in each event registering a fake candidate.

tor of the original incident particle, s is the shower age ($s = 1$ being the shower maximum) and N_i is the number of particles of species i in the shower. This parameterization has been validated in realistic simulations from CORSIKA, see Fig 1. This approach neglects some sources of systematic uncertainty, such as the hadronic interaction model, dependence on the atmospheric conditions, and dependence of ρ on the initial particle species.

We use an unbinned likelihood to extract incident particle energy and direction:

$$L(N, \theta, \phi) = \prod_i P_0(x_i, y_i) \prod_j P_1(x_j, y_j)$$

where the i index runs across phones that did not reconstruct a candidate and the j index runs across phones that did reconstruct a candidate. The symmetric use of phones with and without candidates naturally handles the non-uniform distribution of deployed phones. In areas of high particle density, the possibility exists of multiple hits on a single phone, allowing for additional power in determining the shower density. We leave this for later refinements.

Expected performance in simulated events drawn from Eq. 1 is shown in Fig. 7 for various scenarios in $A\epsilon$ and phone density. The resolution improves with higher shower energy due to higher statistics from an increased particle density. Lower values of $A\epsilon$ can be compensated by higher phone densities, as shown by the overlapping curves.

The background, due to electronic noise, uncorrelated muons and ambient radioactivity, is not expected to be correlated among phones. Requiring a 5-phone coincidence within a 5s time window gives an expected non-coincident background rate of 1% of phones.

Energy resolution is very important, as the lower-energy showers appear at a much higher rate than the higher-energy showers of interest. Figure 8 shows that the reconstructed shower energy is not biased by the presence of fake clusters, those due to noise or uncorrelated backgrounds. Even for fake-cluster rates as high as 10% of active phones, much larger than the expected rate, the energy resolution for very high-energy showers is largely unaffected by fake clusters and spurious showers composed of pure background events are negligible above 10^{17} eV. The fraction of reconstructed showers with energy significantly higher than the true incident particle energy is also measured to be small.

Expected Observational Power

The per-shower efficiency is calculated in simulation by sampling randomly placed phones in the path of a shower and determining the number of phones which register a hit. If at least five phones register a hit, the shower is labeled as found; see Fig. 9. The per-shower efficiency is then the fraction of showers which have at least five phones registering hits. The per-shower efficiency rises with incident particle energy due to the increase in the number of particles in the shower. The expected rate per area per year is the incident flux [22] integrated over energy bins and multiplied by the per-shower efficiency, see Fig 10; we assume a field of view of 1.7π sr, corresponding to a zenith range of $0 - 80^\circ$. The dominant contribution at all angles is from muons, due to their much larger efficiency, despite their rarity with respect to photons in vertical showers.

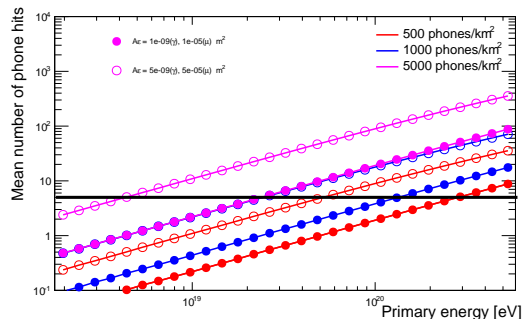


FIG. 9: Mean number of phones registering particle hits per shower and expected observational rates versus incident primary particle energy, for two choices of per-phone area times efficiency ($A\epsilon$) and three examples of user adoption density.

The observing power of state-of-the-art dedicated ground arrays is determined by the *exposure*, which is the product of the observing area, the field of view and the length of the data-taking period. For Auger, the current exposure is approximately 4×10^4 km² sr yr [22] over

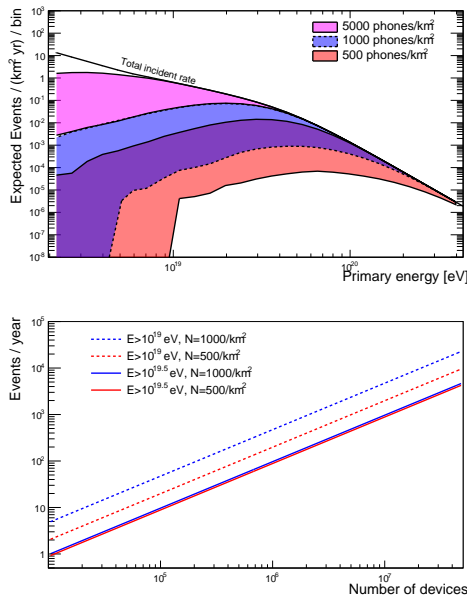


FIG. 10: Top pane: expected number of observed events from UHECRs per year in one square kilometer, as a function of the incident particle energy for three examples of user adoption density. Also shown is the total expected incident rate for a detector with unit efficiency, from a fit to Auger data [22]. The width of the bands indicates the uncertainty in the per phone efficiency ϵ and sensor area A . Bottom pane: expected number of observed events globally as a function of the number of devices. The user density can be compared to the population density of Manhattan ($25,000/\text{km}^2$) or Los Angeles ($3000/\text{km}^2$).

a period from 2004-2012, corresponding to an effective instantaneous exposure of approximately $4.4 \times 10^3 \text{ km}^2 \text{ sr}$. To achieve a similar instantaneous exposure with a network of smartphones with a field of view of $1.7\pi \text{ sr}$ would require an instrumented area of about 825 km^2 . Under the optimistic per-phone $A\epsilon$ scenario, a network of 1000 phones in a square kilometer approaches 100% shower detection efficiency for UHECRs above $10^{19.5} \text{ eV}$. Therefore, 825k phones clustered into 825 groups, each with 1000 phones within a square kilometer, would achieve such an exposure. Note that this assumes continuous operation; some degradation of observational power is expected, as phones will typically join the network during night-time charging. The observational power of such a network clearly hinges on the level of user adoption and continued participation.

A large network of devices would have unprecedented observing power at energies above 10^{20} eV , where current ground arrays become saturated [22]. Lack of observations of UHECRs above this energy could therefore provide powerful limits on the incident flux.

Such a world-wide network of devices sensitive to muons and photons could also have many other potential uses, such as monitoring local radiation levels. In

addition, such a global network would be the first of its kind, opening a new observational window to unanticipated processes.

Conclusions

We propose a novel strategy for observing air showers due to ultra-high energy cosmic rays: an array composed of smartphones running a dedicated app. We have measured the per-phone sensitivity to the particles which comprise the showers and estimated the number of phones needed to achieve observing power to rival the most sensitive current observatories.

Building an installed user base of more than 1M devices operating reliably poses a social and organizational challenge. We have begun to address these by reducing the barriers to participation via automatic and inobtrusive operation, and providing incentives for users.

Acknowledgements

We thank Davide Gerbaudo, Tatiana Rodriguez, Josh Cogliati, Rocky Dendo, Steve Barwick, Gourang Yodh, Kyle Cranmer, Jonathan Wallick for useful conversations, alpha testing and source calibration.

-
- [1] J. Abraham et al. (Pierre Auger Collaboration), *Astropart.Phys.* **29**, 188 (2008), 0712.2843.
 - [2] J. Abraham et al. (Pierre Auger Collaboration), *Science* **318**, 938 (2007), 0711.2256.
 - [3] A. R. Bell, *Mon.Not.Roy.Astron.Soc.* **182**, 147 (1978).
 - [4] R. Blandford and D. Eichler, *Phys.Rept.* **154**, 1 (1987).
 - [5] E. Waxman, *Phys.Rev.Lett.* **75**, 386 (1995), astro-ph/9505082.
 - [6] T. J. Weiler, *Astropart.Phys.* **11**, 303 (1999), hep-ph/9710431.
 - [7] R. Abbasi et al. (High Resolution Fly's Eye Collaboration), *Phys.Rev.Lett.* **92**, 151101 (2004), astro-ph/0208243.
 - [8] M. Takeda, N. Hayashida, K. Honda, N. Inoue, K. Kadota, et al., *Phys.Rev.Lett.* **81**, 1163 (1998), astro-ph/9807193.
 - [9] J. Abraham et al. (Pierre Auger Collaboration), *Phys.Rev.Lett.* **101**, 061101 (2008), 0806.4302.
 - [10] K. Greisen, *Phys.Rev.Lett.* **16**, 748 (1966).
 - [11] G. Zatsepin and V. Kuzmin, *JETP Lett.* **4**, 78 (1966).
 - [12] A. Aab et al. (Telescope Array Collaboration, Pierre Auger Collaboration), *Astrophys.J.* (2014), 1409.3128.
 - [13] N. Hayashida et al. (AGASA Collaboration), *Astropart.Phys.* **10**, 303 (1999), astro-ph/9807045.
 - [14] URL <http://www.ergotelescope.org/>.
 - [15] J. J. Cogliati, K. W. Derr, and J. Wharton (2014), 1401.0766.
 - [16] A. R. Smith, R. J. McDonald, D. C. Hurley, S. E. Holland, D. E. Groom, W. E. Brown, D. K. Gilmore, R. J.

- Stover, and M. Wei, in *Sensors and Camera Systems for Scientific, Industrial, and Digital Photography Applications III*, edited by M. M. Blouke, J. Canosa, and N. Sampat (2002), vol. 4669 of *Society of Photo-Optical Instrumentation Engineers (SPIE) Conference Series*, pp. 172–183.
- [17] URL <http://crayfis.ps.uci.edu/>.
- [18] D. Heck, G. Schatz, T. Thouw, J. Knapp, and J. Capdevielle (1998).
- [19] S. Ostapchenko, Phys.Rev. **D83**, 014018 (2011), 1010.1869.
- [20] S. Agostinelli et al. (GEANT4), Nucl.Instrum.Meth. **A506**, 250 (2003).
- [21] P. Grieder, *Extensive Air Showers* (Springer, 2010).
- [22] A. Aab et al. (Pierre Auger Collaboration) (2013), 1307.5059.